American Journal of Mechanical and Materials Engineering
2021; 5(4): 83-91
http://www.sciencepublishinggroup.com/j/ajmme
doi: 10.11648/j.ajmme.20210504.15
ISSN: 2639-9628 (Print); ISSN: 2639-9652 (Online)

Effect of Surface Texture on the Steady-state Characteristics of Journal Bearing and Its Comparisons

Ashutosh Rajput, Lintu Roy

Department of Mechanical Engineering, National Institute of Technology Silchar, Assam, India

Email address:
lintu2003@gmail.com (L. Roy)

To cite this article:
Ashutosh Rajput, Lintu Roy. Effect of Surface Texture on the Steady-state Characteristics of Journal Bearing and Its Comparisons. *American Journal of Mechanical and Materials Engineering*. Vol. 5, No. 4, 2021, pp. 83-91. doi: 10.11648/j.ajmme.20210504.15

Received: November 25, 2021; **Accepted**: December 14, 2021; **Published**: December 24, 2021

Abstract: The journal bearing has been an important mechanical part of the mechanical system, and over the decade's researchers have been investigating how to analyse and enhance its performance. In order to improve the bearing performance, the surface texture and texture shape have the potential to improve its performance efficiently. Therefore, the present paper investigates the effect of different types of texture such as elliptical, cylindrical for the steady-state characteristics of journal bearing. It has been found that the incorporation of texture on the inner side surface of the bearing has a significant influence on the steady-state characteristics of the bearing. The resultsare obtained in terms of non-dimensional Sommerfeld number (S), attitude angle (ϕ), friction variable (μ), and flow coefficient (q_z), by using the finite difference method and Gauss-Seidel method. The successive over-relaxation (SOR) technique has been applied to satisfy the boundary conditions. The obtained reluts show the improvement in tribological performance of the bearing characteristics through incorporation of texture. In addition, a comparative analysis of textured bearings i.e., elliptical, cylindrical is also done withplain journal bearing. It has been investigated that elliptical surfacestexturehas superior performance in contrast to cylindrical and plain textures.

Keywords: Hydrodynamic Lubrication, Dimple Textured Journal Bearing, Finite Difference Method

1. Introduction

Journal bearings are used in several mechanical components like industrialtools, automobiles etc. The function of the bearing is to carry the load while the shaft is rotated inside it. Many researchers [1-3] have reported that the performance of bearing significantly improves by introducing the texture on the inner side of the bearing. Therefore, it is necessary to examine the potential use of texturing and its various form of geometrical shape for improving the performance of the hydrodynamic journal bearing. The performance of the bearing can be analysed by load-carrying capacity, attitude angle, friction co-efficient and flow coefficient.

Etsion [1] reviewed the worldwide effortson surface texture and suggested that laser surface texturing (LST) can be used as a promising technology for developing the textures on the surface of the bearing. The study also highlighted the fundamental ongoing research around the world on LST. Priest and Taylor [2] believed that the technology of surface texturing is expected to be important for futuristic bearing structure design. Wakuda [3] analyse the effect of micro-dimples on the frictional properties for that Pin-on-disk tests is conducted. Two tests have been carried out, one for a lapped smooth surface with texture another for a lapped smooth surface without texture. In a lapped smooth surface with the textured sample, the size and shape of dimples are varying in addition to alteration in dimple density. A substantial reduction in frictional coefficient is reported from 0.12 to 0.10 [3]. Sinanoglu et. al. [4] examine the pressure and load bearing capacity of journal bearing, in which journal/shaft surface is textured. Two shape one saw and another is trapezoidal are considered in the texturing of the shaft surface. It has been examined that trapezoidal profile textured shat can carry more load than the saw profile textured shaft. Both experimental and nural network techniques considered in the analysis of pressure and load [4]. Uehara et. al. [5] performed the block on ring friction test under oil lubricant. The dimple on the block has been prepared with abrasive jet machining. During the test, optimization of friction with the dimple, s density is carried out for 40μm dimple size and found that below 7.5% dimple density, the friction remains as usual but at 15% dimple

density friction reduced significantly. When the dimple density increases above 15% dimple density increase in friction are observed. Kovalchenko et al.[6] has performed the pin-on-disk test to observe the LST effect under high sliding speed and found that the friction coefficient is lower on the textured surface than the polish surface. The adhesion of thin-film lubricant with the polish surface is reported as a cause for higher friction in the polish surface. The LST has a profound effect at higher sliding speed in high viscous lubricant and a significant reduction in friction coefficient is also reported in the investigation [6]. Sinanoglu [7] is investigated the tribological performance of threaded texture shaft surfaces by experimental and theoretical neural network approaches. It is suggested that the screw thread act as a hydrodynamic bearing and micro-reservoir. The screw thread supplies the lubricant in starved lubricant condition. It has been found that the load-bearing capacity is substantially enhanced in a certain degree of threaded textured shaft surface than shaft surface without texture. Rahmani et. al. [8] have performed the analytical study of slider bearing with textures surface. three shapes are considered in the study like rectangular, triangular rectangular, and isosceles triangular. It has been noted that the shape and type of texture can significantly affect the performance of the bearing [8]. Two parameters i.e., optimum height and textured area ratio are considered for the investigation. The optimisation has been performed to set the optimum texturing parameter for evaluating the maximum load capacity, minimum friction, and load capacity to lubricant flow rate [8]. Tala-Ighil et al. [9] examine the bearing characteristics for cylincrical textured journal bearing theoretically. The study analysed the bearing characteristic under three different conditions, partially textured full textured and deep textured. It has been observed that full texturing is ineffective and can not lift the shaft through the hydrodynamic effect due to the cavitation effect [9]. However, partially texture bearing can lift the shaft when texturing is done on the decline part of hydrodynamic pressure. Moreover, the deep texture gives the maximum bearing performance at the eccentricity ratio of 0.6 when declined part of the pressure field is textured [9]. Cupillard et. al. [10] analysed the inertia effect of fluid on textured hydrodynamics contacts. In the analysis, textured depth is optimised and critical depth of textured is set, above the critical textured depth negative inertia effect is obtained below this critical textured depth positive inertia effect is noted. However, high load carrying capacity is found high at the optimum textured depth, which is relatively greater than the critical textured depth. It is also noted that above the optimum texture load carrying capacity decreases significantly due to the finding of the recirculation zone [10]. **S.** Kango et. al. [11] analysed the performance of micro-texture journal bearing under the combined effect of heat dissipation and non-Newtonian rheological lubricant. The performance has been analysed using the mass conservation algorithm (JFO boundary condition) and found more realistic results in the JFO boundary condition than the Reynolds boundary condition. Gupta et. al [12] analysed the textured hydrodynamic journal bearing, experimentally. The texture is prepared with help of a mechanical indentation technique on the inner side of the journal bearing surface and a large tribological data is captured for investigatingthe comparative analysis between smooth and textured journal bearing. the result of analysed data shows higher tribological for texture journal bearing [12]. Qui et. al. [13] analysed the textured parallel sliding surface lubricated with gaseous lubricants. Various textured shapes i.e., spherical, ellipsoidal, circular, elliptical, triangular, and chevron-shaped dimples are considered while analyzing the tribological performance of the bearing. The compressible Reynolds equation is solved to obtain the pressure distribution and load carrying capacity for the domain having ten dimples. Additionally, the geometry of the textures and the texture density is optimised as a function of operating parameters i.e., relative velocity and space between the sliding surfaces. The ellipsoidal shape texture on the sliding surface results in maximum load-carrying capacity [13]. Reddy and Kakoty [14] use the elliptical texture on the journal bearing surface to evaluate the performance of the journal bearing. The analysis suggested a significant improvement in the tribological performance of the journal bearing with elliptical texture. The analysis reported an increase in flow co-efficient and reduction in friction variables [14]. Malik and Kakoty [15] investigated the performance of parallel and inclined slider bearings in which the surface of the slider bearing has been constructed with the dimpled texture. The simple non-dimensional technique is used in the analysis, and the textured directionality effect has been taken into consideration. The improvement in bearing performance is noted in the forward texturing, and on the contrary, lower bearing performance is indicated in backward texturing [15].

Based on the above literature survey, surface texturing emerges as a usable option for enhancement in the performance of the journal bearing. Therefore, the analysis of journal bearing is performed in the presence of textures (circular, cylindrical and elliptical) on the inner side of the bearing. The texture journal bearing performance has been evaluated in terms of non-dimensional parameters such as pressure distribution, Sommerfeld number, attitude angle, friction coefficient, and flow co-efficient and comparison has been drawn for plain, cylindrical textured, and elliptical textured journal bearing.

2. Analytical Model

Figure 1 shows a schematic view of plain hydrodynamic journal bearing. In Figure 1(a), the shaft is located at the inner side of the journal, the journal center is O and its radius is R. The shaft carries the load 'W', therefore, it has been shifted eccentrically at 'O_1'and the eccentricity is 'e' and radius of the shaft is 'r'. The thickness of lubricant film is 'h', and it helps in building the hydrodynamics pressure between tribological components such as the journal and shaft. The film thickness is varying from position 'θ =0' to position 'θ =π'. The position 'θ =0' represents where the film

thickness is maximum and '$\theta = \pi$' illustrates the place where the film thickness is minimum. The angle 'ϕ' is the angle between the line passing from the 'O' and 'O_1' and the line passing from the normal load 'W'. Figure 1(b) illustrate the texture grid, which is situated at the inner side of the journal. The base radius of the dimple is 'r_p'. The grid cell dimensionsare 'r_1'and 'r_2' in the horizontal and vertical directions, respectively. The dimension 'L' represents the length of the cell and the dimension '$\theta = \pi$' represents the circumferential length of the textured region. The symbolsX and Z represent the horizontal and vertical coordinates, respectively.

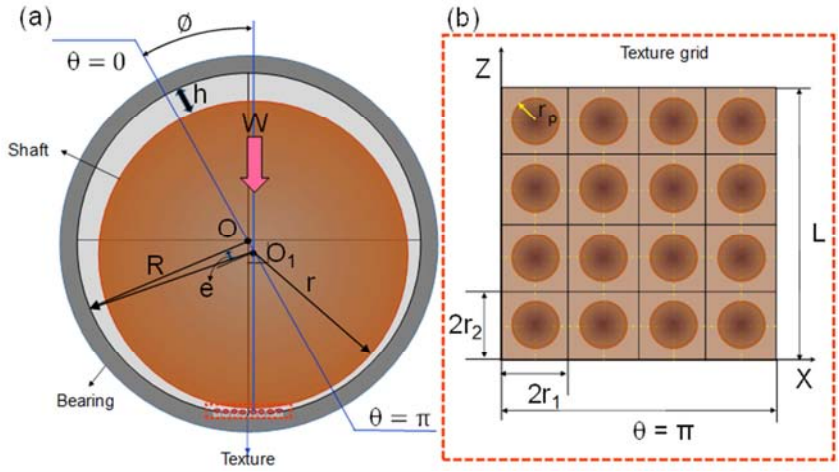

Figure 1. *(a) Schematic view of hydrodynamic journal bearing. (b) the theoretical model of surface textured journal bearing in the cartesian coordinates form, located at the inner journal bearing.*

A theoretical model has been developedto study the journal bearing properties for a textured surface consisting of dimples as shown in figure 1(b). For developing the model, the steady-state classical Reynolds equation is applied for evaluating the pressure distribution and it is given as follows

$$\frac{\partial}{\partial x}\left(\frac{\rho h^3}{12\eta}\frac{\partial p}{dx}\right)+\frac{\partial}{\partial z}\left(\frac{\rho h^3}{12\eta}\frac{\partial p}{\partial z}\right)=u\frac{\partial(\rho h)}{\partial x} \qquad (1)$$

where 'ρ' is fluid density 'η' is the fluid viscosity, 'h' is the film thickness, and 'u' represents the journal velocity. For obtaining the non-dimensional form of the Reynolds equation following parameters have been used as given below

$$x = r_p * \bar{x},\ z = r_p * \bar{z},\ h = h_o * \bar{h},\ \bar{P} = \frac{1}{\Lambda}\frac{P}{P_a},\ \Lambda = \frac{3\rho\eta U}{2r_p P_a}$$

After putting the above parameters in equation (1), the equation (1) can be converted into the non-dimensional form, as given below

$$\frac{\partial}{\partial \bar{x}}\left(\bar{h}^3\frac{\partial \bar{P}}{\partial \bar{x}}\right)+\frac{\partial}{\partial \bar{z}}\left(\bar{h}^3\frac{\partial \bar{P}}{\partial \bar{z}}\right)=\frac{1}{\delta^2}\frac{\partial \bar{h}}{\partial \bar{z}} \qquad (2)$$

The non-dimensional equation (2) is used in the calculation of pressure distribution over the bearing area. The pressure is investigated in two directions, one is parallel and another is normal to the centerline of the bearing.

2.1. Texture Parameters

To consider the geometrical effect of bearing, the bearing geometries are converted into a non-dimensional form. The following parameters have been used in converting the non-dimensional form, as given below,

$$\delta = \frac{c}{2r_p},\ \bar{h}_p = \frac{h_p}{c},\ \bar{x} = \frac{x}{r_p},\ \bar{x} = \frac{x}{r_p},\ \bar{x}^* = \frac{x^*}{r_p},\ \bar{z}^* = \frac{z^*}{r_p},$$
$$\bar{L} = \frac{L}{r_p},\ \bar{R} = \frac{R}{r_p},\ \bar{h} = \frac{h}{c},\ \psi = \frac{h_p}{2r_p}$$

2.2. Texture Density

Eventually, the textures are patterned over the inner side of the bearing surface. It has been considered that the geometry and shape of the texture are identical to each other, hence the base radius 'r_p" and texture depth 'h_p' respectively are the same for all the textures. As shown in Figure 1(b) the texture is located at the center of the cell having the area ($2r_1$*$2r_2$). To analyse the influence of the texture area density (S_p), the area density (S_p) of the texture is calculated, as given below:

$$S_p = \frac{\pi r_p^{\,2}}{2r_1 \times 2r_2},\ \text{where } r_1 = k \times r_2$$

$$S_p = \frac{\pi \times r_p^{\,2}}{4 \times k \times r_2^{\,2}},\ \text{where } \bar{r} = \frac{k \times r_2}{r_p} \qquad (3)$$

$$\bar{r} = \frac{1}{2}\sqrt{\frac{\pi}{S_p}}$$

Figure 2 represents the side view of the spherical shape dimple, which is used to find the fluid film thickness (h) at any point in the textured surface. From figure 2.

$$BD = r_p,\ OD = OA = r,\ AB = h_p,\ O'B = c,$$
$$OO' = \left[OA - \left(O'B + BA\right)\right],\ OO' = r - \left(c + h_p\right)$$

Form the figure 2ΔOBD

$$\left(r - h_p\right)^2 + {r_p}^2 = r^2,\ \text{now}\ r = \frac{{r_p}^2 + {h_p}^2}{2h_p} \tag{4}$$

$$OO' = \left[\frac{{r_p}^2 + {h_p}^2}{2h_p} - \left(c + h_p\right)\right]$$

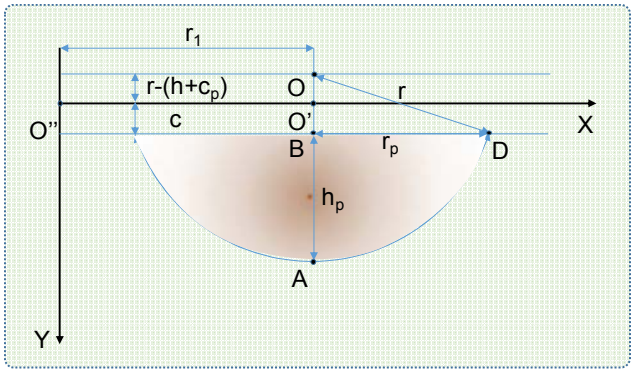

Figure 2. *Geometry for circular Texture.*

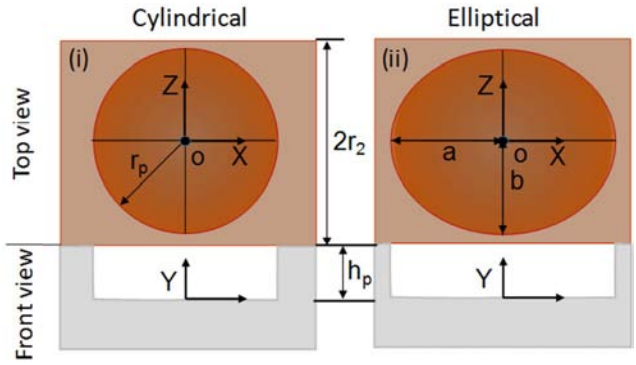

Figure 3. *Texture geometries (i) For Cylindrical and (ii) circular (h_p=0) and (b) For Elliptical.*

Now the sphere equation of radius 'r' is:

$$x^2 + y^2 + z^2 = r^2$$

By transferring the co-ordinate of the system from O to O' in Figure 2 the following equation has been obtained as:

$$y = \sqrt{r^2 - \left(x - r_1\right)^2 - \left(z - r_2\right)^2} - \left[r - \left(c + h_p\right)\right] + e\cos\theta \tag{5}$$

Substituting the value 'r' from equation (4) intheabove equation.

$$y = c + e\cos\theta + h_p - \left(\frac{{r_p}^2 + {h_p}^2}{2h_p}\right) + \sqrt{\left(\frac{{r_p}^2 + {h_p}^2}{2h_p}\right) - \left(x - r_1\right)^2 - \left(z - r_2\right)^2}$$

when $\left(x - r_1\right)^2 + \left(z - {r_2}^2\right) \le {r_p}^2$

Where c is clearance, h_p is maximum dimple depth, and e represents the eccentricity.

2.3. Film Thickness

The film thickness is varying from angle '0' to 'π' and it is influenced by texture depth. The expression for film thickness with texture depth is given as follows:

$$h = c + e\cos\theta + h_p - \left(\frac{{r_p}^2 + {h_p}^2}{2h_p}\right) + \sqrt{\left(\frac{{r_p}^2 + {h_p}^2}{2h_p}\right) - x^{\circ 2} - z^{*2}}$$

When

$$x^{*2} + z^{*2} \le {r_p}^2 \tag{6}$$

$$h = c + e\cos\theta \text{ when } x^{*2} + z^{*2} > {r_p}^2$$

where x^* and z^* are the local coordinatesof the circle and its origin coincides with the imaginary cell center.

Now the expression for local dimensionless film thickness can be obtained after substituting the non-dimensional parameter.

$$\bar{h} = 1 + \varepsilon\cos\theta + \bar{h}_p - \left(\frac{1}{8\delta^2\bar{h}_p} + \frac{\bar{h}_p}{2}\right) + \sqrt{\left(\frac{\bar{h}_p}{2} + \frac{1}{8\delta^2\bar{h}_p}\right)^2 - \frac{1}{4\delta^2}\left(\bar{x}^{*2} + \bar{z}^{*2}\right)}$$

$$\bar{h} = 1 + \varepsilon\cos\theta + \left(\frac{1}{8\delta\psi} - \frac{\psi}{2\delta}\right) + \sqrt{\left(\frac{\psi}{2\delta} + \frac{1}{8\delta\psi}\right)^2 - \frac{1}{4\delta^2}\left(\bar{x}^{*2} + \bar{z}^{*2}\right)} \text{ when } \bar{x}^{*2} + \bar{z}^{*2} \le 1 \tag{7}$$

$$\bar{h} = 1 + \varepsilon\cos\theta \text{ when } \bar{x}^{*2} + \bar{z}^{*2} > 1 \tag{8}$$

Where $\bar{x}^{*2}$ and $\bar{z}^{*2}$ are localdimensionless length and width,$\bar{h}$ is the dimensionless local height, $\overline{h_p}$ is dimple depth, and δ represents dimensionless clearance.

2.4. Steady State Characteristic of a Texture Journal Bearing

To evaluate the bearing load, dimensionless pressure is integrated over the bearing area. Therefore pressure has been integrated along the axial direction and normal of the bearing.

$$W\cos\varphi = -2\bar{R}\int_0^{\bar{L}/2}\int_0^{2\pi}\bar{p}\cos\theta.d\theta.d\bar{z} \tag{9}$$

$$W\sin\varphi = -2\bar{R}\int_0^{\bar{L}/2}\int_0^{2\pi}\bar{p}\sin\theta.d\theta.d\bar{z}\ ;$$

$$\tan\varphi = \frac{2\bar{R}\int_0^{\bar{L}/2}\int_0^{2\pi}\bar{p}\sin\theta.d\theta.d\bar{z}}{-2\bar{R}\int_0^{\bar{L}/2}\int_0^{2\pi}\bar{p}\cos\theta.d\theta.d\bar{z}} \tag{10}$$

The dimensionless load-carrying capacity can be obtained by normalizing the dimensional load 'W' into the non-dimensional load $\bar{W}$. the equation for dimensionless load-carrying can be written as

$$W = \Lambda P_a r_p{}^2\bar{W} \tag{11}$$

The load-bearing capacity of the journal can be obtained in terms of classical Sommerfeld number which can be written as

$$S = \frac{\eta UL}{\pi W}\left(\frac{R}{c}\right)^2 \tag{12}$$

The dimensionless form of the Sommerfeld number can be obtained from (12) by using the parameter Λ, δ, $\bar{L}$ and $\vec{R}$ after rearranging the parameters the Sommerfeld Number can be written as

$$S = \frac{\bar{L}}{6\pi\bar{W}}\left(\frac{\bar{R}}{\delta}\right)^2 \tag{13}$$

2.5. Boundary Conditions

The following boundary condition has been used to solve the non-dimensional Reynolds equation written as follows

$$\left.\begin{matrix}\bar{p}(\theta=0,\bar{z})=0\\ \bar{p}(\theta=\grave{\theta},\bar{z})=0\\ \bar{p}(\theta,z=0)=0\end{matrix}\right\}$$

$$\frac{\partial\bar{p}}{\partial\bar{z}}\left(\theta,z=\frac{\bar{L}}{2}\right)$$

The first three conditions written in the enclosed bracket represent that the local pressure $\bar{p}$ at the inlet $(\theta=0)$, local pressure $\bar{p}$at the initial cavitations site is given by$(\theta=\grave{\theta})$, and at the bearing boundary $z=0$ to the ambient pressure p_a corresponding to non-dimensional pressure $\bar{p}$. The following boundary condition is because of the symmetry of the problem concerningthe middle plane z=L/2.

The value of 'θ' at the beginning of the cavitation zone "θ"" is unknown. Therefore the basic boundary condition has been completed by the Reynolds equation

$$\frac{d\bar{p}}{d\theta}(\theta=\theta')=0$$

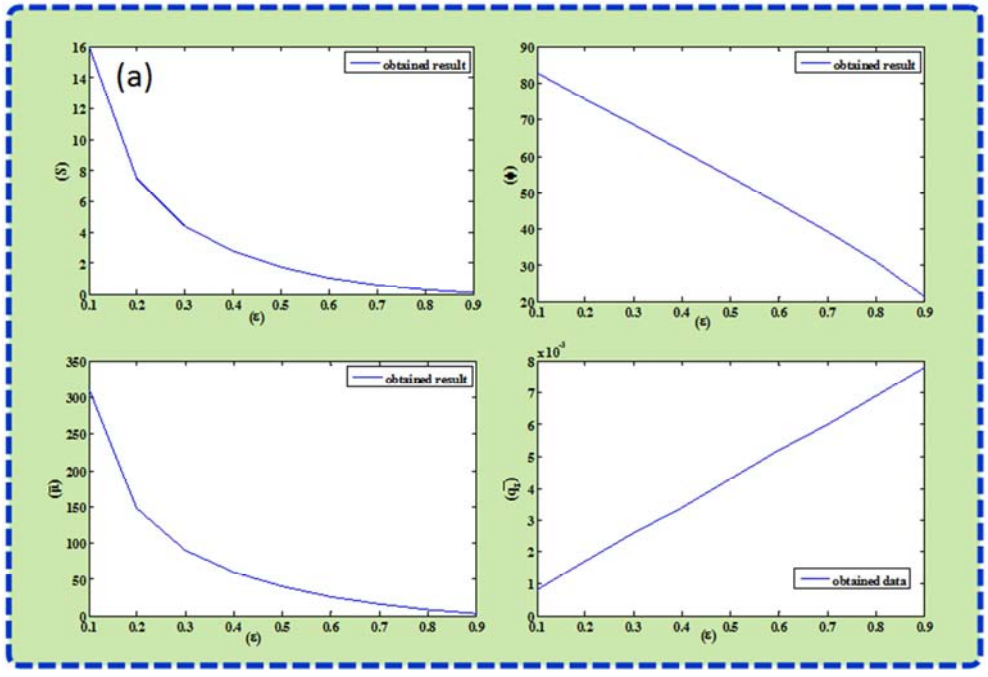

Figure 4. *Variation of tribological parameter with with eccentricity ratio for l/d=1, area-density (s_p)=0.5, and texture depth (h_p)=0.0: (a) Sommerfeld number, (b) Attitude angle, (c) Friction variable, and (d) Flow co-efficient.*

3. Results and Discussion

3.1. Elliptical Texture Journal Bearing

The results for elliptical textured journal bearing is drawn in Figure 4. The tribological parameters Sommerfeld number, attitude angle, friction coefficient, and flow co-efficient are plotted with varying eccentricity ratios at constant area density (s_p)=0.5, dimple height (h_p)=0.01 and aspect ratio (l/d)=1. As shown in Figure 1(a), the Sommerfeld number decreases exponentially with an increasing eccentricity ratio. The reduction in the Sommer field number (S) illustrates the enhancement in the load-bearing capacity because of Sommer feld number is inversely proportional to the applied load. The attitude angle reduces with increasing the eccentricity ratio, as shown in Figure 1(b). Like the sommer feld number, the behaviour of the friction coefficient is also found similar and it is decreases with increasing the eccentricity ratio, as depicted in Figure 4(b). However, the fluid flow coefficient increases with increases the eccentricity. The behaviour of fluid flow co-efficient is almot linear with eccentricity in the given range.

3.2. Variation of Bearing Characteristics with Texture Depth (h_p)

The texture depth has a significant influence on the tribological parameters. The results of dimensionless load capacity, attitude angle, friction coefficient, and fluid co-efficient are represented with increasing texture depth (h_p) for constant l/d ratio 0.25, area-density (s_p) 0.5 and eccentricity ratio 0.6, as shown in Figure 5. As shown in Figure 5(a), that the load-carrying capacity increases with increasing the texture depth, the behaviour of load carrying capacity is almost linear with dimple textured depth. In addition to that, the attitude angle is also increased with increasing the texture depth, as depicted in Figure 5(b). However, the friction coefficient decreases with increases the texture depth in the given range of texture depth. Moreover, it can be noted from Figure 5(d) that the fluid flow coefficient increases with increasing the texture depth. Respective results of tribological parameters are found consistent with results reported in the literature [15].

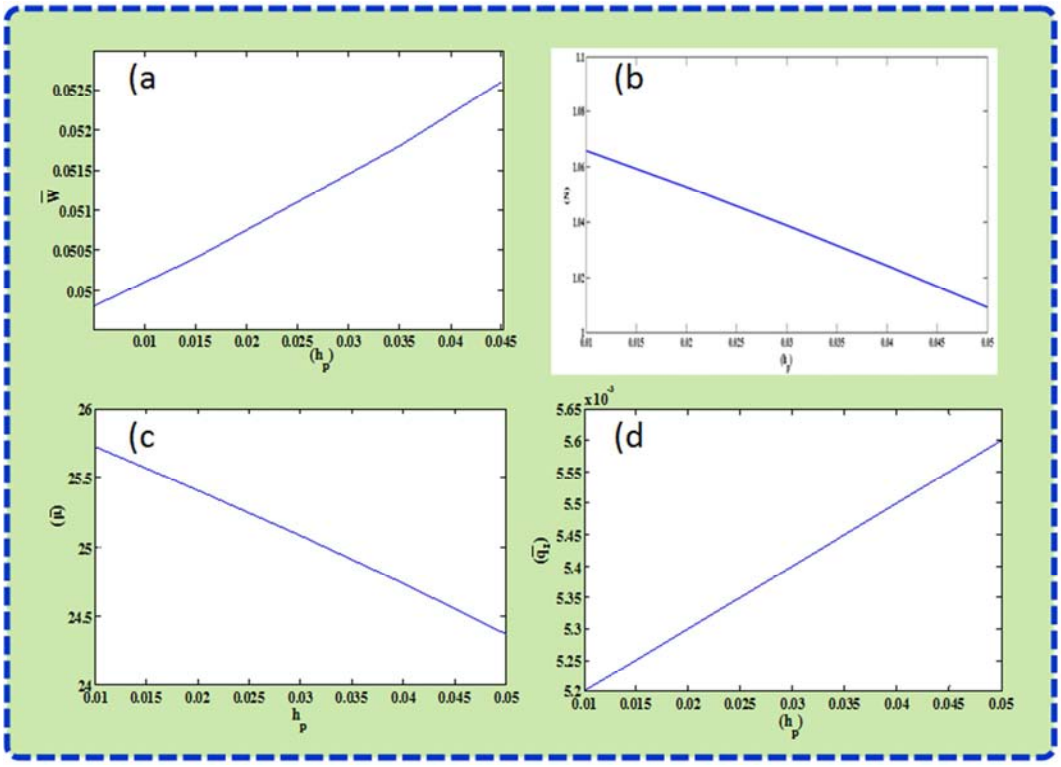

Figure 5. *Variation of tribological parameter with texture depth for L/D=0.25 area-density (s_p)=0.5 and eccentricity=0.6: (a) attitude angle () non dimensional load (c) friction variable, and (d) flow co-efficient.*

3.3. Comparative Analysis of Bearing Characteristics for Elliptical, Cylindrical Texture Journal Bearing with Plain Journal Bearing

The comparison of pressure profiles for the elliptical and cylindrical textured journal bearing and plain journal are drawn in Figure 6. The pressure profile has been drawn at the constant aspect ratio (L/D) of 0.25, dimple height is 0.01, dimple area density (s_p) is 0.5, and eccentricity ratio (ε) is 0.1. It can be been analysed from Figure 6 that the peak of pressure is maximum for elliptical texturing concerning the cylindrical and plain journal bearing. However, the peak of non-dimensional pressure for the cylindrical textured journal is also found high than the plain journal bearing. The higher peak in

elliptical textured journal bearing indicates higher pressure bearing capacity than cylindrical and plain journal bearing.

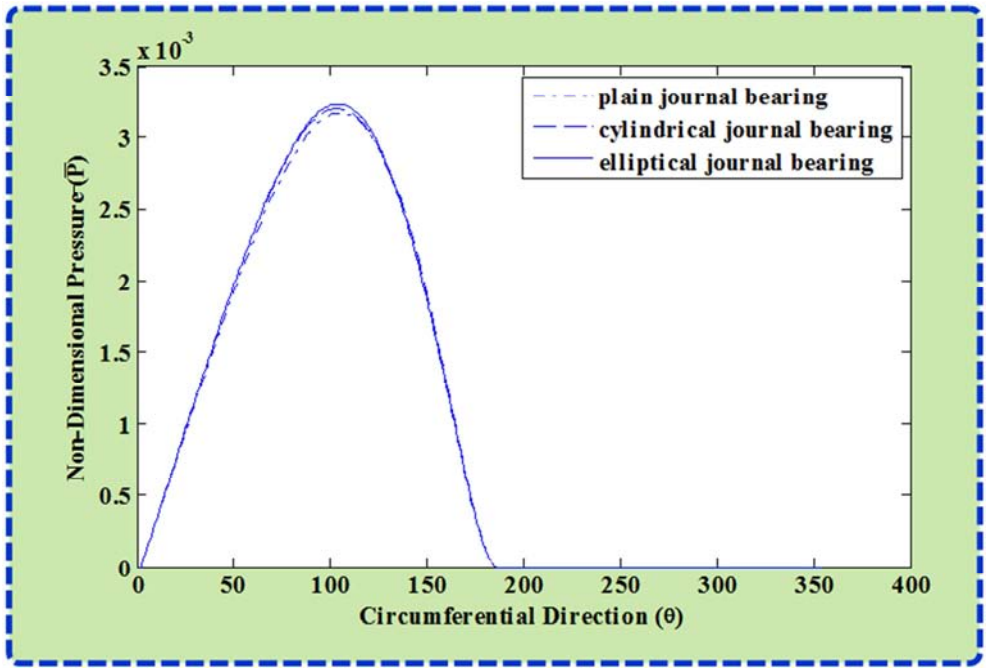

Figure 6. *Pressure distribution curve for elliptical, cylindrical, circular and plain journal bearing for aspect ratio (L/D)=0.25, dimple height 0.01, dimple area density (s_p)=0.5, and eccentricity ratio (ε)=0.1.*

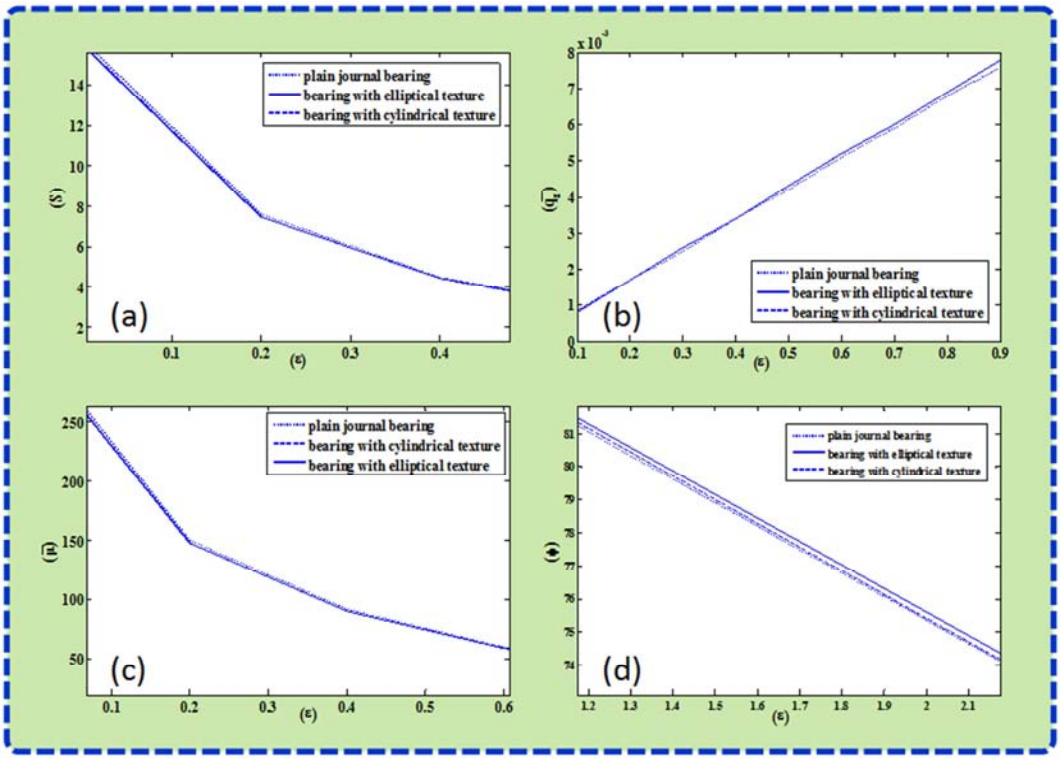

Figure 7. *Comparison of tribological parameters for plain, cylindrical, and elliptical journal bearing at the aspect ratio (L/D)=0.25, dimple height 0.01, dimple area density (s_p)=0.5, and eccentricity ratio (ε)=0.1. and at the is varying eccentricity ratio. (a) Sommerfeld Number (S), (b) attitude angle, (c) friction variable, and (d) Variation of flow co-efficient with eccentricity ratio.*

Figure 7 illustrates the comparative analysis of elliptical, cylindrical, and plain journal bearing. The results are obtained as Sommerfeld number (S), friction coefficient ($\bar{\mu}$) and attitude angle (ϕ), fluid co-efficient ($\overline{q_z}$) at constant (L/D)=0.25, dimple height 0.01, dimple area density (s_p)=0.5. and eccentricity ratio (ε)=0.1. Although, the behaviour of Sommerfeld number with eccentricity ratio is the same for all the journal bearing., but its value for pain journal bearing is

relatively high. As shown in Figure 7(a), its value for elliptical and cylindrical journal bearing is almost the same for the given range of eccentricity.

Figure 7(b) describes the flow co-efficient and computation has been drawn to distinguish the behaviour of elliptical, cylindrical, and plain journal bearing. The behaviour of flow co-efficient with eccentricity ratio is almost the same, and its value continuously increases with increasing the eccentricity ratio. but its value for elliptical and cylindrical journal bearing is the same and higher than the plain journal bearing.

Figure 7(c) describes the behaviour of friction co-efficient with eccentricity ratio, and a comparison has been drawn for elliptical, cylindrical, and plain journal bearing. As it can be observed from the that the value of friction decreases with increasing eccentricity ratio. The value of friction coefficient is noted higher in plain journal bearing than the elliptical and cylindrical journal bearing.

Figure 7(d) shows the response of attitude angle with eccentricity ratio, and it can be observed from that its value continuously decreases with increases the eccentricity ratio. A similar trend is noted for all the journal bearing i.e., elliptical, cylindrical, and plain journal bearing. However, its value for elliptical journal bearing is high and low for plain journal bearing and remains moderate for cylindrical journal bearing.

Table 1. *The comparison of present results with existing results available in the literature [9].*

Steady-state Characteristic	Cylindrical Texture bearing	Elliptical Textured bearing	N Tala-Ighil [9]
Load Capacity	12881N	12731N	12600N
Sommerfeld Number	0.1184	0.1198	0.1210
Eccentricity Ratio	0.600	0.600	0.601
Attitude Angle	50.2498	50.6427	50.4

3.4. Validation of the Result for Texture Journal Bearing

The table has been drawn below to validate the obtained results with the existing data available in the literature [9]. For the validation tribological parameters such as load capacity. Sommerfeld number (S), eccentricity ratio, and attitude angle are compared. The performance of cylindrical and ellipitical journal bearing is almost matching and results looks consistent when it is correlated with the results of [9].

4. Conclusion

The sdudy invstigated the tribologocal performance of journal bearing. It has been considered that the bearing surface is textured with ellipitical, cylindrical and comparisions have been drawn for elliptical, cylindrical textured bearing and plain journal bearing. Based on the above analysis following conclusions are drawn given below:

1. It has been noted that the Sommerfeld number (S), attitude angle (ϕ), friction coefficient ($\bar{\mu}$) decreases with increases the eccentricity ratio, incontrast to that flow co-efficient ($\overline{q_z}$) increases with increasing the eccentricity ratio.
2. Dimple depth has significant influence on tribological performance therefore the tribological performance has been also evaluated with dimple texture depth. It is observed that load-carrying ($\bar{W}$) capacity, fluid flow coefficient ($\overline{q_z}$), increases with increasing texture depth, contrary, friction coefficient ($\bar{\mu}$) and Sommerfeld feld number (S) decreases with the same.
3. The tribological performance improves with incorporation of texture on the bearing surface. The perfomane of the textured bearing is found higher than the plain journal bearing. However the performace of the ellipiticl and cylindrical textured bearing is almost same.
4. The dimensionless pressure distribution of journal bearing is found higher with elliptically textured surface than theclylindrical and plain surface.

Nomenclature

R	radius of journal (m)
$\bar{R}$	dimensionless bearing radius
D	diameter of the bearing
L	length of bearing (m)
$\bar{L}$	dimensionless bearing length
p	local pressure
$\bar{p}$	dimensionless local pressure
p_a	ambient pressure
C	radial clearance (m)
e,ε	eccentricity (m), eccentricity ratio $\varepsilon = e/C$
N	journal rotation speed (rpm)
ω	journal angular speed (rad/s_
U	linear speed of moving surface (m/s)
W	radial load
$\bar{W}$	dimensionless load capacity
x, y, z	co-ordinates
x^*, y^*	local coordinates
$\bar{x}, \bar{z}$	dimensionless co-ordinates
$\overline{x^*}, \overline{z^*}$	dimensionless local co-ordinates
$h(x, z)$	local film thickness
$\bar{h}$	dimensionless local film thickness
h_p	dimple depth (m)
$\bar{h}_p$	dimensionless dimple depth
r_p	dimple base radius in meter
S_p	area density
Λ	bearing number
δ	dimensionless bearing clearance
Ψ	dimple aspect ratio
θ	angle in the circumferential direction
S	Sommerfeld number

References

[1] Etsion, Izhak. "State of the art in laser surface texturing." *J. Trib.* 127, no. 1 (2005): 248-253.

[2] Priest, M., and Christopher Mark Taylor. "Automobile engine tribology—approaching the surface." *Wear* 241, no. 2 (2000): 193-203.

[3] Wakuda, Manabu, Yukihiko Yamauchi, Shuzo Kanzaki, and Yoshiteru Yasuda. "Effect of surface texturing on friction reduction between ceramic and steel materials under lubricated sliding contact." *Wear* 254, no. 3-4 (2003): 356-363.

[4] Sinanoğlu, Cem, Fehmi Nair, and M. Baki Karamış. "Effects of shaft surface texture on journal bearing pressure distribution." *Journal of materials processing technology* 168, no. 2 (2005): 344-353.

[5] Uehara, Y., M. Wakuda, Y. Yamauchi, S. Kanzaki, and S. Sakaguchi. "Tribological properties of dimpled silicon nitride under oil lubrication." *Journal of the European Ceramic society* 24, no. 2 (2004): 369-373.

[6] Kovalchenko, Andriy, Oyelayo Ajayi, Ali Erdemir, George Fenske, and Izhak Etsion. "The effect of laser texturing of steel surfaces and speed-load parameters on the transition of lubrication regime from boundary to hydrodynamic." *Tribology Transactions* 47, no. 2 (2004): 299-307.

[7] Sinanoglu, Cem. "Investigation of load carriage capacity of journal bearings by surface texturing." *Industrial Lubrication and Tribology* (2009).

[8] Rahmani, Ramin, Iraj Mirzaee, Ayoub Shirvani, and Hassan Shirvani. "An analytical approach for analysis and optimisation of slider bearings with infinite width parallel textures." *Tribology International* 43, no. 8 (2010): 1551-1565.

[9] Tala-Ighil, Nacer, Michel Fillon, and Patrick Maspeyrot. "Effect of textured area on the performances of a hydrodynamic journal bearing." *Tribology International* 44, no. 3 (2011): 211-219.

[10] Cupillard, Samuel, Sergei Glavatskih, and M. J. Cervantes. "Inertia effects in textured hydrodynamic contacts." *Proceedings of the Institution of Mechanical Engineers, Part J: Journal of Engineering Tribology* 224, no. 8 (2010): 751-756.

[11] Kango, S., R. K. Sharma, and R. K. Pandey. "Thermal analysis of microtextured journal bearing using non-Newtonian rheology of lubricant and JFO boundary conditions." *Tribology International* 69 (2014): 19-29.

[12] Gupta, K. Kumar, Raj Kumar, Harendra Kumar, and Medha Sharma. "Study on effect of surface texture on the performance of hydrodynamic journal bearing." *International Journal of Engineering and Advanced Technology* 3, no. 1 (2013): 49-54.

[13] Qiu, Mingfeng, Adis Delic, and Bart Raeymaekers. "The effect of texture shape on the load-carrying capacity of gas-lubricated parallel slider bearings." *Tribology Letters* 48, no. 3 (2012): 315-327.

[14] Ganji, T. S., S. K. Kakoty, and R. K. Pandey. "Analysis on micro elliptical textured journal bearing." *International Journal of Current Engineering and Technology* 2, no. 2 (2014): 648-650.

[15] Malik, Surajit, and Sashindra K. Kakoty. "Analysis of dimple textured parallel and inclined slider bearing." *Proceedings of the Institution of Mechanical Engineers, Part J: Journal of Engineering Tribology* 228, no. 12 (2014): 1343-1357.